

Contents

W.G. van der Wiel <i>et al.</i> / Photon Assisted Tunneling in Quantum Dots	2
--	---

PHOTON ASSISTED TUNNELING IN QUANTUM DOTS

W.G. VAN DER WIEL, T.H. OOSTERKAMP,
S. DE FRANCESCHI, C.J.P.M. HARMANS
AND L.P. KOUWENHOVEN

*Department of Applied Physics and DIMES, Delft University
of Technology, PO Box 5046, 2600 GA Delft, The Netherlands*

We review experiments on single-electron transport through single quantum dots in the presence of a microwave signal. In the case of a small dot with well-resolved discrete energy states, the applied high-frequency signal allows for inelastic tunnel events that involve the exchange of photons with the microwave field. These photon assisted tunneling (PAT) processes give rise to sideband resonances in addition to the main resonance. Photon absorption can also lead to tunneling via excited states instead of tunneling via the ground state of the quantum dot. The manipulation of quantum dots by a microwave field is an important ingredient for the possible application of quantum dots as solid state quantum bits, which forms a motivation for this review.

1. Introduction

Transport properties of quantum dots at zero frequency have been extensively studied and by now many aspects are well understood [1]. In some studies finite, but still low frequency signals were applied to a gate electrode nearby the quantum dot. Capacitance spectroscopy on quantum dots has been performed at kHz frequencies [2]. At MHz frequencies, quantum dots can be operated as turnstiles or pumps [3]. These frequencies, f , are low in the sense that the photon energy, hf , is much smaller than the thermal energy, $k_B T$, and thus the discrete photon character cannot be discerned. For sufficiently high frequencies, such that $hf \gg k_B T$, the interaction of the electromagnetic field with the electrons confined in a quantum dot would be analogous to light spectroscopy studies on atoms. However, different quantum dots are not microscopically equal. The response of an ensemble of quantum dots to light excitation is therefore strongly averaged. Despite this averaging, excitation studies on arrays of quantum dots by far-infrared light

(i.e. the THz regime) have revealed the spectrum of collective modes [4], i.e. the sloshing modes of the whole electron puddle in the external potential. Excitations within the electron puddle are difficult to create since, according to the generalized Kohn theorem [4], the dipole field of far-infrared radiation does not couple to the relative coordinates of electrons confined in a parabolic quantum dot. This problem is circumvented by inelastic light scattering experiments which have been able to detect electronic excitations in arrays of quantum dots that can be related to a discrete single-particle spectrum [5]. Recently, this technique has also probed excitons in a single quantum dot [6].

In this review, we discuss electron transport experiments on single quantum dots, that are irradiated by a microwave signal. In contrast to light transmission, luminescence, or inelastic light scattering measurements (see for a review Ref. [7]), we measure the dc current in response to a microwave signal. Current can flow through a quantum dot when a discrete energy state is aligned to the Fermi energies of the leads. This resonant current is carried by elastic tunneling of electrons between the leads and the dot. An additional time-varying potential $\tilde{V} \cos(2\pi ft)$ can induce *inelastic* tunnel events when electrons exchange photons of energy hf with the oscillating field. This inelastic tunneling with discrete energy exchange is known as photon assisted tunneling (PAT). Microwave studies have a long tradition in the field of superconductor-insulator-superconductor tunnel junctions [8], for which the theory was first described by Tien and Gordon in 1963 [9]. Despite many proposals and a long search [10], it took thirty years before PAT was also observed in a non-superconducting system. In 1993 PAT features were seen in the current-voltage characteristics of a GaAs/AlGaAs superlattice under THz irradiation from a free-electron laser [11]. Starting in 1994, PAT was also found in experiments on single-electron transport through semiconductor quantum dots [12-16]. The quantum dots in Ref. [13] were rather large and effectively had a continuous density of states. Here, we focus on PAT processes through quantum dots with well-resolved, discrete energy states. For these small dots, the resonant tunneling peak in the current develops photon sideband resonances when we apply microwaves [16]. The energy separation between main peak and sidebands can be used as a spectroscopic measurement of the energy levels in the dot.

The relevant ac regime for quantum dots is at much lower frequency than visible light. We list the important frequency scales in Table I. The single-particle level spacing $\Delta\varepsilon$ is 0.05 - 0.5 meV for typical dots and the charging energy, e^2/C , is usually 0.2 - 2 meV. To observe effects from a finite $\Delta\varepsilon$ and e^2/C , these energies should exceed the thermal broadening $\sim 4k_B T$. Other characteristic frequencies of the dot are related to the transport times. Γ is the typical rate to tunnel on or off the dot, which can be arbitrarily small for

opaque tunnel barriers. This frequency is set by the transmission coefficient of the barriers and should be kept smaller than $\Delta\varepsilon$ otherwise the level broadening exceeds the spacing between the single-particle states. The final time scale is the tunneling time; i.e. the actual time spent during tunneling through the barrier. This time is quite short (~ 2 ps) for typical barriers (calculated within the Büttiker-Landauer framework [17]). To access these time scales, ac signals can be applied, and the effects on the dc transport can be measured.

TABLE I. A list of the important energy/frequency scales for transport through quantum dots. For $f = 10$ GHz the photon energy, hf , is $40 \mu\text{eV}$.

Quantity	Equivalent frequency	Typical frequencies
Thermal broadening	$\sim 4k_B T/h$	10 GHz (at 100 mK)
Tunneling rate on/off the dot	Γ	0 - 100 GHz
Level spacing (or inverse traversal time)	$\Delta\varepsilon/h$	10 - 100 GHz
Charging energy	e^2/hC	40 - 400 GHz
Tunneling time	$1/\tau_{\text{tunnel}}$	200 GHz - 1 THz

If $f \ll \Gamma$ each electron sees an essentially static potential and we are in the adiabatic regime [2, 18]. If $f \gg \Gamma$, each electron experiences many cycles of the ac signal while it is on the dot; i.e. the non-adiabatic regime. If $hf \ll 4k_B T$, single photon processes are masked by thermal fluctuations, and a classical description is appropriate [3]. Thus, the discreteness of the photon energy can be observed in the non-adiabatic, high-frequency regime: $hf \gg h\Gamma, 4k_B T$. This is the quantum, or time-dependent regime for which it is essential to solve the time-dependent Schrödinger equation for the tunneling electron.

This review is divided into two parts. First, in section 2, we discuss the theory of PAT through a single junction (2.1) and calculations of PAT through a single quantum dot using a master equation approach (2.2). Numerical PAT calculations are presented in sections 2.3 and 2.4. Second, in section 3, we discuss experimental results of PAT measurements on single lateral quantum dots. The sample geometry is discussed in section 3.1, the sensitivity of pumping to the applied microwave frequency in 3.2. PAT in the low ($hf < \Delta\varepsilon$) and high frequency ($hf > \Delta\varepsilon$) regime are discussed in 3.3 and 3.4, respectively. In sections 3.5 through 3.7 results are given of the

dependence of PAT on microwave frequency, magnetic field and microwave power, respectively. We conclude and discuss the results in section 3.8.

2. Theory

2.1. PAT THROUGH A SINGLE JUNCTION

First, we briefly outline photon assisted transport through a single tunnel junction separating two metallic leads. An oscillating potential difference across a junction, $\tilde{V} \cos(2\pi ft)$, where \tilde{V} is the ac amplitude, may be included in the Hamiltonian of one of the leads as: $H = H_0 + H_{ac} = H_0 + e\tilde{V} \cos(2\pi ft)$, where the unperturbed Hamiltonian, H_0 , describes the leads without microwaves. The effect of the oscillating potential is that the time-dependent part of the electron wave function in this lead, when expanded into a power series, contains energy components at E , $E \pm hf$, $E \pm 2hf$, ..., etc. These are called sidebands. The expansion can be done as follows [9]:

$$\begin{aligned} \psi(r, t) &= \varphi(r) \exp \left(-i \int dt [E + e\tilde{V} \cos(2\pi ft)] / \hbar \right) \\ &= \varphi(r) \exp(-iEt/\hbar) \sum_{n=-\infty}^{\infty} J_n(e\tilde{V}/hf) \exp(-in2\pi ft) \\ &= \varphi(r) \left(\sum_{n=-\infty}^{\infty} J_n(e\tilde{V}/hf) \exp(-i[E + nhf]t/\hbar) \right) \end{aligned} \quad (1)$$

$\varphi(r)$ is the eigenfunction satisfying $H_0\varphi(r) = E\varphi(r)$ and forms the spatial part of the wave function $\psi(r, t)$. $J_n(\alpha)$ is the n th order Bessel function of the first kind (see Fig. 1a) evaluated at $\alpha = e\tilde{V}/hf$.

Let ρ_l and ρ_r be the unperturbed densities of states of the left and right leads. The tunnel current through a junction without a microwave field is then given by

$$I(V_{SD}) = c \int_{-\infty}^{\infty} dE [f_l(E - eV_{SD}) - f_r(E)] \rho_l(E - eV_{SD}) \rho_r(E) \quad (2)$$

where V_{SD} is the source-drain voltage, $f(E)$ is the Fermi function, and c is a constant proportional to the tunnel conductance.

From Eq. (1), we can write an effective density of states in one of the leads (we choose the right lead) given by:

$$\tilde{\rho}_r(E) = \sum_{n=-\infty}^{\infty} \rho_r(E + nhf) J_n^2(e\tilde{V}/hf) \quad (3)$$

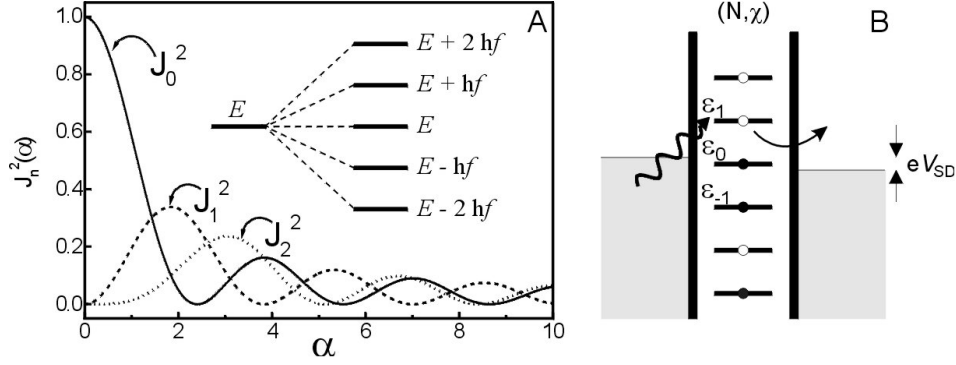


Figure 1. (a) Squared Bessel functions of the first kind $J_n^2(\alpha)$, for $n = 0, 1$ and 2 . The inset shows the development of sidebands of the original energy as a consequence of the microwave field. The population probability $P(n)$ of the different sidebands is given by $P(n) = J_n^2(e\tilde{V}/hf)$. A positive or negative n corresponds to the absorption or emission, respectively, of n photons during the tunnel process. Elastic tunneling corresponds to $n = 0$. (b) Schematic energy diagram of a single dot containing N electrons distributed over the available single-particle levels ε_j in a particular configuration χ . By absorption of a photon, an electron can tunnel into ε_1 so that the electron number changes into $N + 1$ and the configuration into χ' .

If tunneling is a weak perturbation, the dc current in the presence of microwaves, \tilde{I} , is given by [9]:

$$\begin{aligned}
 \tilde{I}(V_{SD}) &= c \sum_{n=-\infty}^{\infty} J_n^2(e\tilde{V}/hf) \times \\
 &\quad \int_{-\infty}^{\infty} dE [f_l(E - eV_{SD}) - f_r(E + nhf)] \rho_l(E - eV_{SD}) \rho_r(E + nhf) \\
 &= \sum_{n=-\infty}^{\infty} J_n^2(e\tilde{V}/hf) I(V_{SD} + nhf/e)
 \end{aligned} \tag{4}$$

We stress that tunneling is assumed to be a weak perturbation, implying that the sidebands are only well-defined for $f \gg \Gamma$. Since there is no electric field in the scattering-free leads, mixing of electron states [19], or photon absorption is absent in the leads. A positive or negative n corresponds to the absorption or emission, respectively, of n photons during the tunnel process. Elastic tunneling corresponds to $n = 0$. *For a single junction the dc current in the presence of microwaves is thus described, simply in terms of the dc current without microwaves.* From the normalization $\sum_{n=-\infty}^{\infty} J_n^2(\alpha) = 1$, it follows that the integrated current does not change due to the oscillating potential: $\int \tilde{I}(V_{SD}) dV_{SD} = \int I(V_{SD}) dV_{SD}$. We emphasize that although

the oscillating field is entirely classical, the interaction with an electron, described by the Schrödinger equation, is only via exchange of *discrete* energy quanta. Equation (4) is only valid for single junctions where the tunneling takes place via a single hop. An extension of Eq. (4) to describe a double junction system is discussed next.

2.2. MASTER EQUATION FOR PAT THROUGH A QUANTUM DOT

Electron transport through double barrier structures is resonant when the Fermi energy of the leads aligns with a discrete energy state between the two barriers. Transport through semiconductor quantum wells are usually well described by non-interacting electron models. Also, their transport properties in the presence of an oscillating signal can, in a first-order approximation, be described by the time-dependent, non-interacting Schrödinger equation. The result of such calculations is that, next to the main resonance, extra peaks appear at distances corresponding to the photon energy, hf [20, 21].

In quantum dots electrons are confined in all directions. The total number of electrons, and the total charge, is thus a discrete value. This makes it essential to include the Coulomb interactions when describing transport. The standard model is known as the single-electron tunneling, or the Coulomb blockade model [22]. This model takes into account that at low voltages and low temperatures only one electron can tunnel at a time. The necessary energy to add an extra electron to a quantum dot consists of the charging energy $E_c = e^2/C$ for a single electron, and a discrete energy difference, $\Delta\varepsilon$, arising from the quantum-mechanical confinement. In practice, a quantum dot has discrete energy states if $\Delta\varepsilon$ exceeds the thermal energy $k_B T$ [1]. Assuming sequential tunneling of single electrons, the current can be calculated with a master equation [23, 24].

PAT through small systems in which Coulomb blockade is important was considered first by Likharev and Devyatov [25], Hadicke and Krech [26], and Bruder and Schoeller [27]. A direct inclusion of the Tien and Gordon equations [9] in a master equation that takes into account Coulomb blockade [22] can be made by writing the tunnel rate through each barrier in the presence of microwaves $\tilde{\Gamma}(E)$ in terms of the rates without microwaves $\Gamma(E)$ [12]:

$$\tilde{\Gamma}(E) = \sum_{n=-\infty}^{+\infty} J_n^2(\alpha) \Gamma(E + nhf) \quad (5)$$

Equation 5 has a direct link to studies of the effects of fluctuations in the electromagnetic environment on single-electron tunneling [28]. If the spectral density of the environment is characterized by the probability function

$P(hf)$, then the rate including the environment $\Gamma_{env}(E)$, can be written in terms of the rate without the environment $\Gamma(E)$ as [29]:

$$\Gamma_{env}(E) = \int_{-\infty}^{\infty} d(hf) P(hf) \Gamma(E + hf) \quad (6)$$

Whereas Eq. (5) describes a monochromatic environment, the fluctuations in general are broad band in frequency, as described in Eq. (6). Examples of environments that have been studied experimentally, are the impedance in the leads [28], blackbody radiation [30], and phonons [31]. We note, however, that Eqs. (5,6) are valid only for systems with a continuous density of states (i.e. $\Delta\varepsilon \ll k_B T$) and immediate relaxation to the ground state after each tunnel event.

In the case of quantum dots with large level separation (i.e. $\Delta\varepsilon \gg k_B T$), one needs to keep track of the occupation probabilities of each discrete state. This increases the amount of bookkeeping, but has the advantage that intra-dot relaxation and excitation processes can be included. In our model [32] for PAT through small dots, we assume $E_c \gg \Delta\varepsilon$, $k_B T$, eV_{SD} , nhf , such that we only need to consider two charge states (i.e. the electron number is either N or $N + 1$) [33]. We neglect level broadening due to a finite lifetime of the electrons on the dot.

A charge state (Fig. 1b) is described by the electron number N , together with the particular occupation of the electrons in the available single-particle levels $\{\varepsilon_j\}$. If N electrons are distributed over k levels, the number of distinct dot configurations, χ , is given by $\binom{k}{N}$. The probability, $P_{N,\chi}$, for state (N, χ) is calculated from a set of master equations given by:

$$\begin{aligned} \dot{P}_{N,\chi} = & \sum_{\chi'} P_{N+1,\chi'} (\Gamma_{l,j_{\chi'}}^{out} + \Gamma_{r,j_{\chi'}}^{out}) \\ & - P_{N,\chi} \sum_{j=empty} (\Gamma_{l,j}^{in} + \Gamma_{r,j}^{in}) \\ & + \sum_{\chi'' \neq \chi} P_{N,\chi''} \Gamma_{\chi'' \rightarrow \chi} - P_{N,\chi} \sum_{\chi''' \neq \chi} \Gamma_{\chi \rightarrow \chi'''} \end{aligned} \quad (7)$$

and the equivalent forms for $\dot{P}_{N+1,\chi'}$. To find a stationary solution, these equations are all set to zero ($\dot{P} = 0$) and solved with the boundary condition:

$$\sum_{\chi} P_{N,\chi} + \sum_{\chi'} P_{N+1,\chi'} = 1 \quad (8)$$

For $N = 2$ distributed over five different single-particle levels $\{\varepsilon_j\}$, there are ten different configurations, χ , yielding ten equations for $\dot{P}_{N,\chi}$ and also ten equations for $\dot{P}_{N+1,\chi'}$.

The first and second term in Eq. (7) correspond to a change in the occupation probability of a certain distribution due to tunneling (the number of electrons on the dot changes). In the first term an electron tunnels out of the dot. Only those rates are taken into account that correspond to an electron tunneling out of state $j_{\chi'}$ that leave the dot in the distribution (N, χ) . In the second term, an electron tunnels onto the dot. One needs to sum over all the states j that are empty when the dot is in configuration χ , because all these events cause a transition from state (N, χ) to a state $(N + 1, \chi')$. $\Gamma_{l,j}^{in}$ and $\Gamma_{l,j}^{out}$ are the tunnel rates through the left barrier in and out of single-particle level j on the dot:

$$\begin{aligned}\Gamma_{l/r,j}^{in}(\varepsilon_j) &= \Gamma_{l/r,j} \sum_n J_n^2(\alpha_{l/r}) f(\varepsilon_j - \frac{C_g}{C} eV_g - nhf + \eta_{l/r} eV_{SD}; T_{l/r}) \quad (9) \\ \Gamma_{l/r,j}^{out}(\varepsilon_j) &= \Gamma_{l/r,j} \sum_n J_n^2(\alpha_{l/r}) [1 - f(\varepsilon_j - \frac{C_g}{C} eV_g - nhf + \eta_{l/r} eV_{SD}; T_{l/r})]\end{aligned}$$

where $\Gamma_{l/r,j}$ is the tunnel rate through the left or right barrier of energy level j . $\alpha_{l/r}$ is the parameter describing the microwave field at the left or right barrier, C_g is the gate capacitance, C is the total dot capacitance, $T_{l/r}$ is the temperature of the left or right lead. $\eta_{l/r}$ is a parameter describing the asymmetry of the dc voltage drop across the two barriers. We assume that the tunnel rates, $\Gamma_{l/r,j}$, do depend on the level index j , but that they are independent of energy.

In the last two terms of Eq. (7), the number of electrons on the dot is fixed, while only the distribution of the electrons over the states changes. This includes effects from relaxation (i.e. intra-dot transitions, $\chi'' \rightarrow \chi$ and $\chi \rightarrow \chi'''$, where the total energy decreases) or excitation inside the dot (i.e. intra-dot transitions, $\chi'' \rightarrow \chi$ and $\chi \rightarrow \chi'''$, where the total energy increases). Below, we take excitation rates equal to zero (i.e. no intra-dot absorption) but, allow for non-zero relaxation rates.

An expression for the dc current can be found by calculating the net tunnel rate through one of the barriers. Using the probabilities $P_{N,\chi}$ and the tunnel rates through the left barrier, this leads to:

$$I = e \sum_{\chi} \sum_{j=\text{empty}} P_{N,\chi} \Gamma_{l,j}^{in} - e \sum_{\chi'} \sum_{j=\text{full}} P_{N+1,\chi'} \Gamma_{l,j}^{out} \quad (10)$$

In the numerical calculations in the next section we take equal ac amplitudes dropping across the left and right barriers; i.e. $\alpha_l = \alpha_r = \alpha$.

2.3. NUMERICAL RESULTS

Figure 2 shows calculations without relaxation between the states in the dot. The inset shows the case for transport through only a single level; $\Delta\varepsilon \gg hf$. Next to the main resonance, side-peaks develop at multiples of hf/e when the microwave power is increased via the parameter α . The broadening of the resonances is due to a finite temperature. In the main figure transport can also occur via excited states; here $\Delta\varepsilon < hf$. Not only side-peaks develop, but also peaks at other gate voltages. These peaks arise due to the interplay between the discrete single-particle states and the photon energy. Their locations are given by $(m\Delta\varepsilon + nhf)/e$ where $m = 0, \pm 1, \pm 2, \dots$ and n is the photon number. Similar simulation results have been reported by Bruder and Schoeller [27].

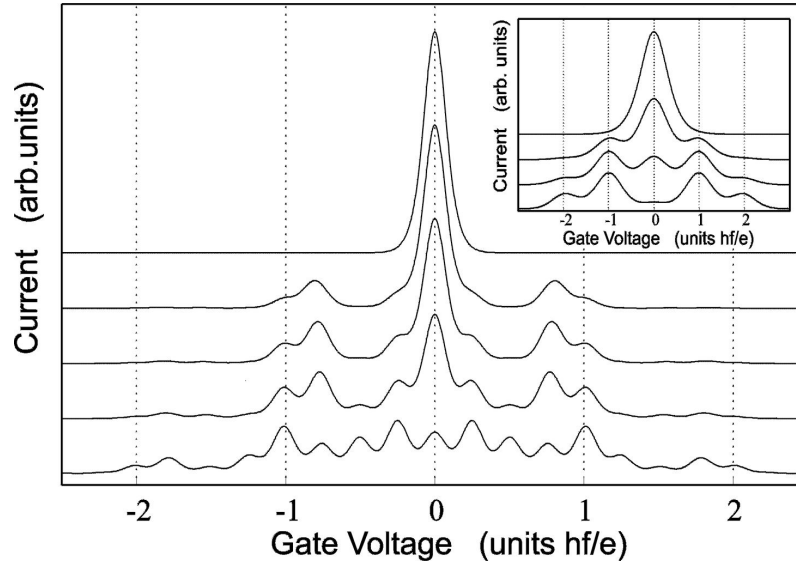


Figure 2. Calculation without relaxation. Curves are offset for clarity. The parameters for the data in the inset are $\Delta\varepsilon = 3hf$, $hf = 5k_B T$, and from top to bottom $\alpha = 0, 1, 1.5, 2$. The parameters for the main figure are $\Delta\varepsilon = 0.75hf$, $hf = 20k_B T$ and from top to bottom $\alpha = 0, 0.5, 0.75, 1, 1.5$.

Figure 3 shows an expansion for the curve with $\alpha = 1$. We have assigned the excited states and the particular PAT processes. The highest occupied single-particle level of the $N + 1$ ground state is denoted by ε_j with $j = 0$; positive j 's are excited states above ε_0 and negative j 's are below ε_0 (see Fig. 1b). The inset shows the effect of relaxation. Upon increasing the relaxation

rate, the peaks corresponding to tunneling through excited states decrease, while peaks increase when tunneling occurs through the ground state.

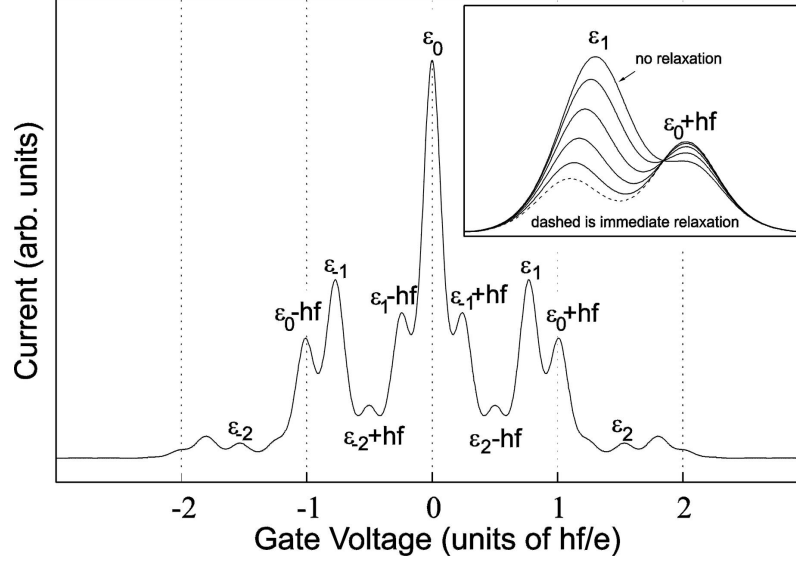


Figure 3. Expansion for the curve $\alpha = 1$ from Fig. 2. The inset shows the effect of an increasing relaxation rate. The relaxation rates divided by the tunnel rate are 0, 0.1, 0.35, 1, 3.5, and infinite.

To explain these numerical results, we show energy diagrams in Fig. 4, assuming that only the highest two single-particle levels contribute to the current for the transition between N and $N + 1$ electrons on the dot. For small dc bias voltage and no ac voltages a current resonance occurs when the topmost energy state (i.e. the electrochemical potential) of the quantum dot lines up with the Fermi levels of the leads (see the diagram ϵ_0). When high-frequency voltages drop across the two barriers, additional current peaks appear. We distinguish two mechanisms. The first mechanism gives photon induced current peaks when the *separation* between the ground state ϵ_0 and the Fermi levels of the leads *matches* the photon energy (or multiples, nhf), as depicted in the diagrams labeled by $\epsilon_0 + hf$ and $\epsilon_0 - hf$. The minus and plus signs correspond to being before or beyond the main resonance. Note that also the case of $\epsilon_0 - hf$ involves photon absorption. Following the literature on the tunneling time, we call these current peaks: *sidebands* [17]. The second mechanism leads to photon peaks when an excited state is in resonance with the Fermi levels of the leads (see diagram ϵ_1). Without PAT, transport through the excited state, ϵ_1 , is blocked since Coulomb blockade prevents having electrons in both the ground state and the excited state

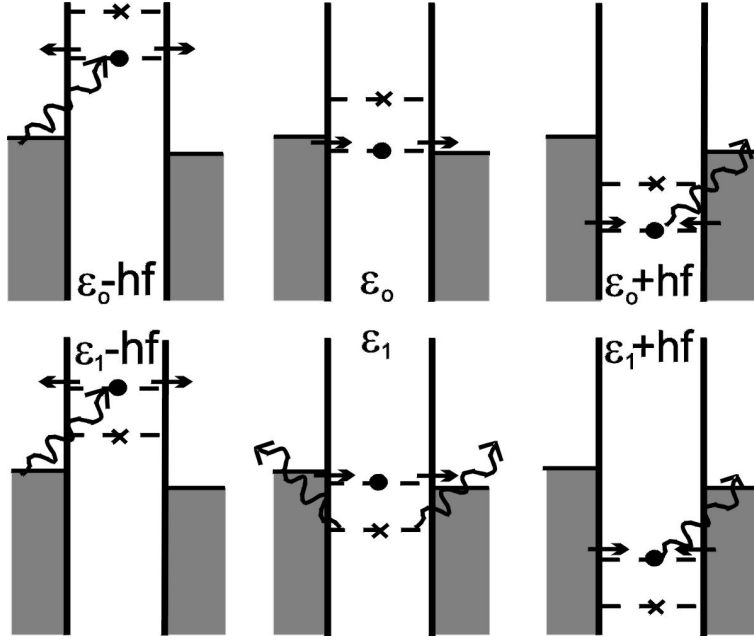


Figure 4. Diagrams depicting the tunneling events which dominantly contribute to the current through a quantum dot at different gate voltages. A small dc bias raises the left Fermi level with respect to the right Fermi level. ε_0 and ε_1 denote the ground state and the first excited state of the $(N+1)$ electron system. When the $(N+1)^{th}$ electron tunnels to one of the two reservoirs, the energy states of the dot drop by the charging energy E_c . The corresponding diagrams for N electrons are not shown.

simultaneously. The electron in the ground state cannot escape from the dot, because its energy is lower than the Fermi levels in the leads. PAT, however, can empty the ground state ε_0 when the electron absorbs enough energy and leaves the dot. This process is analogous to photo-ionization. Now, the $(N+1)^{th}$ electron can tunnel resonantly via the excited state ε_1 as long as the state ε_0 stays empty. Note that for this second mechanism nhf has to *exceed*, but not necessarily *match* the energy splitting $\Delta\varepsilon = \varepsilon_1 - \varepsilon_0$. It is clear from these diagrams that relaxation from ε_1 to ε_0 decreases the height of this resonant peak. More photon peaks are generated when these two mechanisms are combined as in the diagrams labeled by $\varepsilon_1 + hf$ and $\varepsilon_1 - hf$. We thus see that PAT can populate the excited states by tunneling between dot and leads. So, even without intra-dot transitions, we can perform photon spectroscopy on discrete quantum dot states.

2.4. PHOTON-ASSISTED PUMPING

It is important to note that in the diagrams of Fig. 4 only processes with tunneling from or to states in the leads close to the Fermi levels contribute to the net current. Tunnel processes that start with an electron in one of the leads from further below the Fermi level are cancelled by an electron from the other lead. However, this is only true when the ac voltage drop

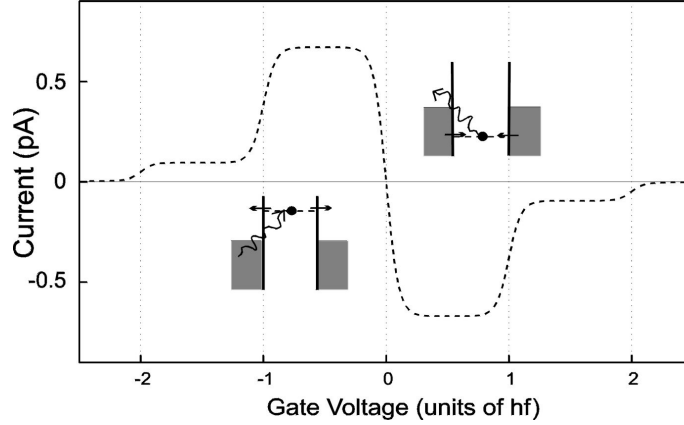


Figure 5. Calculation of the current for zero-bias voltage ($V = 0$) as a function of gate voltage in the case where the ac voltage drop over one barrier is 5% smaller than over the other barrier ($k_B T = 0.05hf$, $\Gamma = 510^8 \text{ s}^{-1}$). The insets depict which tunneling events are responsible for the pumped current when the ground state of the quantum dot is below or above the Fermi levels of the leads.

is the same for both barriers. When the ac voltage drops across the two barriers are unequal, the dot acts as an electron pump [3, 12, 27]. The resulting pumped current makes the resonances discussed above less clear. For this reason we discuss this pumping mechanism in more detail here before proceeding further. Figure 5 shows a calculation of the pumped current as a function of the gate voltage that occurs when the ac voltage drop over one barrier is 5% smaller than over the other barrier. We have taken zero dc bias voltage. To illustrate the origin of the pumped current, the insets show the extreme case, when all the ac voltage drop is across the left barrier. In this case photon absorption occurs only at the left barrier. At negative gate voltage, when the ground-state level of the dot is *above* the Fermi level of the leads, an electron can *enter* the dot from the left lead only (bottom left inset to Fig. 5). Once the electron is in the dot, it can tunnel out through both tunnel barriers. Only tunneling to the right lead contributes to the net current. Therefore, the net (particle) current is to

the right. When the ground-state level of the dot is *below* the Fermi level of the leads, however, an electron can only *leave* the dot to the left lead (upper right inset to Fig. 5). The dot can be filled from either lead once it is emptied. This time only the electron tunneling *in* from the right lead contributes to the net current. Therefore, there is a net current to the left. The difference between these two situations is the shift in the ground-state energy with respect to the Fermi levels of the leads. So, when the gate voltage is swept such that the ground state moves through these Fermi levels, the pumped current changes sign. The pumped current occurs over a width corresponding to the photon energy. The extra shoulders at the far left and far right are due to two-photon processes.

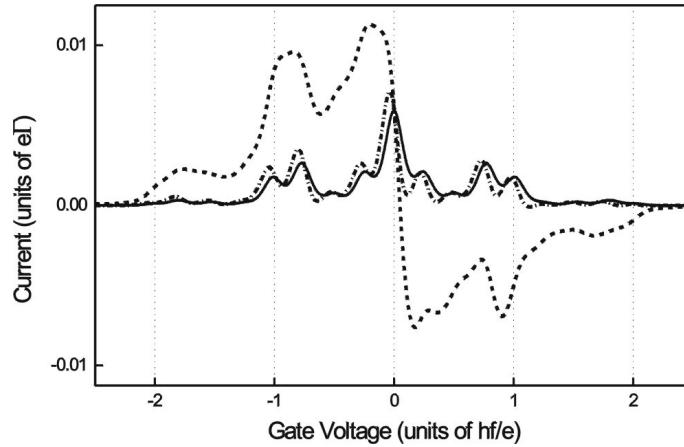


Figure 6. Simulation of the effects of both asymmetric heating and quantum rectification on the curve with $\alpha = 1$ from Fig. 3. The solid line represents the unperturbed curve. The dashed-dotted line shows the same curve for $T_R/T_L = 0.95$. The dashed line shows the influence of $\alpha_R/\alpha_L = 0.95$ on the unperturbed curve.

Asymmetric heating may induce a difference in the temperatures T_R and T_L of the two leads. This can also result in a finite transport current. The effects of asymmetric heating and asymmetric coupling of the microwave signal when a finite V_{SD} is applied across the sample, is illustrated in Fig. 6. The solid line is a reproduction of Fig. 3. The dashed-dotted line shows the same trace for $T_R/T_L = 0.95$. The dashed line shows the influence of $\alpha_R/\alpha_L = 0.95$. It can be concluded that both effects can severely distort the data. At small V_{SD} the resonant peaks scale linearly with V_{SD} , while the pumped current does not change. Increasing the bias, while remaining in the linear regime, therefore improves the visibility of the resonant peaks.

3. Experiments

3.1. SAMPLE GEOMETRY

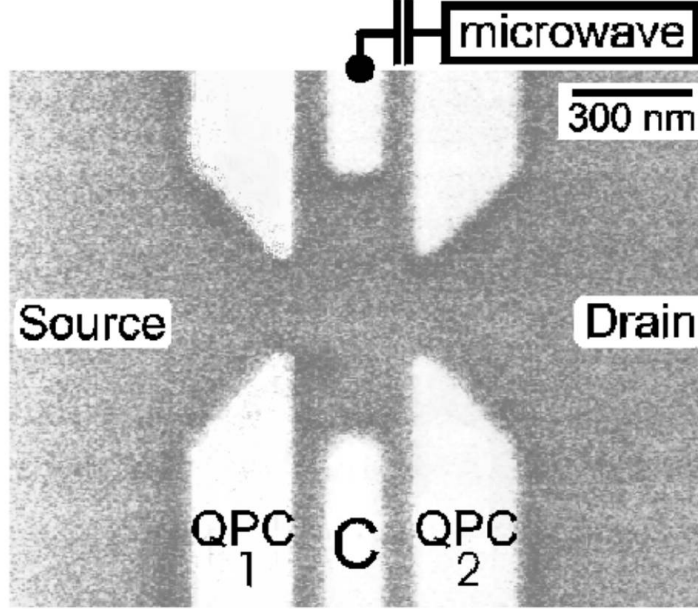


Figure 7. SEM photo of the sample. The lithographic size of the dot is $(600 \times 300) \text{ nm}^2$. Current can flow when we apply a voltage between source and drain. The microwave signal is capacitively coupled to one of the center gates.

Our measurements are performed on a quantum dot defined by metallic gates (see Fig. 7) in a GaAs/AlGaAs heterostructure containing a 2-dimensional electron gas (2DEG) 100 nm below the surface. The 2DEG has mobility $2.3 \cdot 10^6 \text{ cm}^2/\text{Vs}$ and electron density $1.9 \cdot 10^{15} \text{ m}^{-2}$ at 4.2 K. By applying negative voltages to the two outer pairs of gates, we form two quantum point contacts (QPCs). An additional pair of center gates between the QPCs confines the electron gas to a small dot. No electron transport is possible through the narrow channels between the center gates and the gates forming the QPCs. The center gate voltage, V_g , can shift the states in the dot with respect to the Fermi levels of the leads and thereby controls the number of electrons in the dot. The energy shift is given by $\Delta E = \kappa \Delta V_g$, with κ defined as the ratio between the dot-gate capacitance and the total capacitance of the dot [1]. A small dc voltage bias is applied between source and drain and the resulting dc source-drain current is measured. From

standard dc measurements we find that the effective electron temperature is approximately $T = 200$ mK and the charging energy $E_c = 1.2 \pm 0.1$ meV. We independently determine the level splitting, $\Delta\epsilon$, for different magnetic fields from current-voltage characteristics. In addition to the dc gate voltages, we couple a microwave signal (10-75 GHz) capacitively into one of the center gates. The microwave does not equally couple to the dot as to the leads, which results in an ac voltage drop over both barriers.

3.2. FREQUENCY SENSITIVITY OF PUMPING

We first present experimental results with a strongly pumped current taken at $B = 1.96$ T for three frequencies around 47.4 GHz (the arrow denotes hf). The dashed line in Fig. 8 is the current without microwaves. For the lowest frequency the current is pumped in one direction, whereas for the

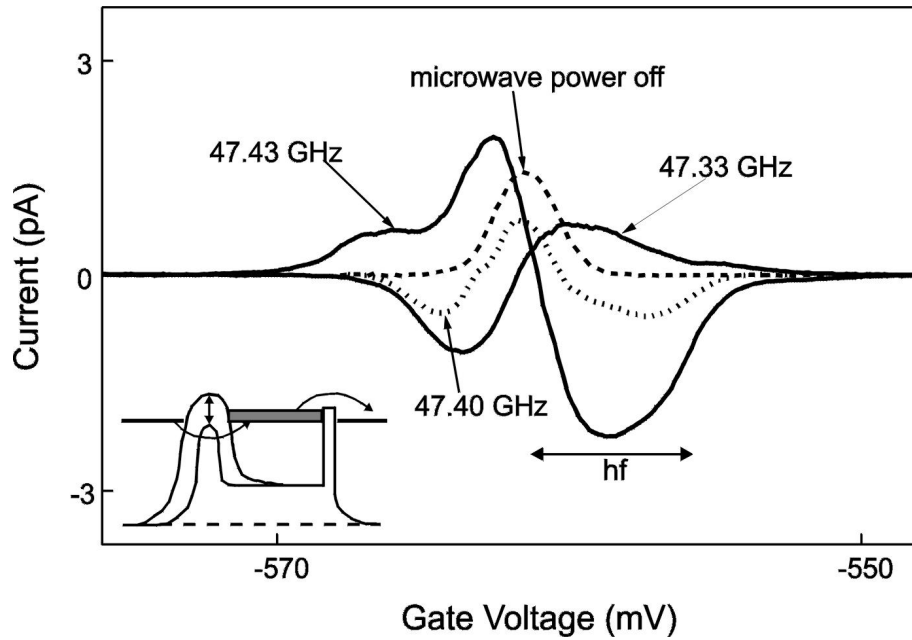


Figure 8. Measurements of the pumped current at $B = 1.96$ T, $V_{SD} = 13$ μ V and frequencies are around 47.4 GHz. Dashed line is without microwaves. The dotted line shows the smallest asymmetry, but shows evidence for a pumping mechanism which is not included in our model.

highest frequency it is pumped in the opposite direction. At 47.33 GHz the left barrier apparently has the *smaller* ac voltage drop, while at 47.43 GHz the left barrier has the *larger* ac voltage drop. This illustrates that the

asymmetry of the voltage drops over the two barriers sensitively depends on frequency. This sensitivity is ascribed to standing waves in the sample holder. The dotted line shows the current measured at an intermediate frequency, where we expect the ac voltage drop to be equal over both barriers. In contrast to the two solid curves, the dotted line is lower than the dashed line without microwaves over the whole gate voltage range. This cannot be explained by the pumping mechanism in our model. Our model only includes the oscillation of the potential of the leads relative to the dot, which always results in a pumped current which changes sign at the resonance. A negative pumped current over the whole gate voltage range, is attributed to the effect of the microwaves on the barrier height. The inset shows how a quantum dot can act as a pump when one tunnel barrier is periodically modulated in height. During one part of the cycle, when the left barrier is low, electrons enter the dot ($\Gamma_L^{low} > \Gamma_R$) while they escape the dot through the right barrier in the second half of the cycle when the left barrier is high ($\Gamma_L^{high} < \Gamma_R$). This is essentially a classical mechanism that has been verified experimentally in the MHz regime [3]. For observing clearly separated PAT sidebands, we first minimize pumping. For this we measure traces of current at zero bias voltage across a single Coulomb peak for slightly different frequencies. We finally choose those frequency values for which the pumped current is very small.

3.3. PAT: LOW FREQUENCY REGIME

First, we study the photon sidebands of the ground state at $B = 0.84$ T [34]. The main part of Fig. 9 shows measured curves of the current as a function of the gate voltage at different microwave powers for the case $hf < \Delta\varepsilon$. Here, current flows primarily via the ground state and its photon sidebands (i.e. upper diagrams in Fig. 4). On increasing the microwave power, we see that the height of the main resonance decreases to zero while additional resonances develop with increasing amplitude. When we convert gate voltage to energy, we find that the additional resonances are located at $\varepsilon_0 \pm hf$ and $\varepsilon_0 \pm 2hf$ [35]. The power dependence is in agreement with the behavior of the Bessel functions: $J_0^2(\alpha)$ for the main resonance ε_0 , $J_1^2(\alpha)$ for the one-photon sidebands $\varepsilon_0 \pm hf$, and $J_2^2(\alpha)$ for the two-photon sidebands $\varepsilon_0 \pm 2hf$. For comparison, we show a calculation in the inset to Fig. 9 for the same values for the temperature, frequency and bias voltage as in the experiment. We have assumed equal ac voltages across the two barriers. The difference between measured and calculated data is attributed to an asymmetry in the ac coupling.

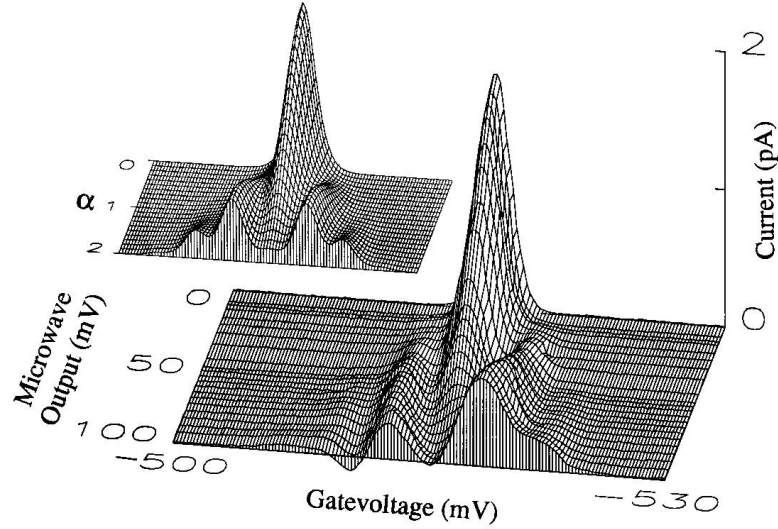


Figure 9. Measurement of the current through the quantum dot as a function of the center gate voltage and the output voltage of the microwave supply. These data are taken in the single-level regime ($hf < \Delta\varepsilon$). $hf = 110 \mu\text{eV}$ for $f = 27 \text{ GHz}$, $\Delta\varepsilon = 165 \mu\text{eV}$ at $B = 0.84 \text{ T}$, and $V_{SD} = 13 \mu\text{V}$. Inset: calculation of the current as a function of the gate voltage and the ac voltage parameter $\alpha = e\tilde{V}/hf$, taking the same values for T , f , and V as in the experiment.

3.4. PAT: HIGH FREQUENCY REGIME

We now discuss the higher frequency regime where $hf > \Delta\varepsilon$, such that PAT can induce current through excited states. Figure 10 shows the current at $B = 0.91 \text{ T}$ (here $\Delta\varepsilon = 130 \mu\text{eV}$). In the top section $f = 61.5 \text{ GHz}$ ($hf = 250 \mu\text{eV}$) and in the bottom section $f = 42 \text{ GHz}$ ($hf = 170 \mu\text{eV}$). As we increase the power, we see extra peaks coming up. We label the peaks as in Fig. 4. On the right side of the main resonance a new peak appears, which we assign to photo-ionization, followed by tunneling through the first excited state. At higher powers the one-photon sidebands of the main resonance as well as those of the excited state resonance appear. We do not observe the peak for $\varepsilon_0 + hf$, in this measurement. This can be explained, at least in part, by the fact that here an electron can also tunnel into ε_1 , which blocks the photon current through $\varepsilon_0 + hf$. Simulations confirm that the peak for $\varepsilon_0 + hf$ can be several times weaker than the peak for $\varepsilon_0 - hf$ [32]. Also, it is masked by the high peak for ε_1 right next to it. The arrows underneath the curves mark the photon energy. The peaks ε_0 and ε_1 remain in place

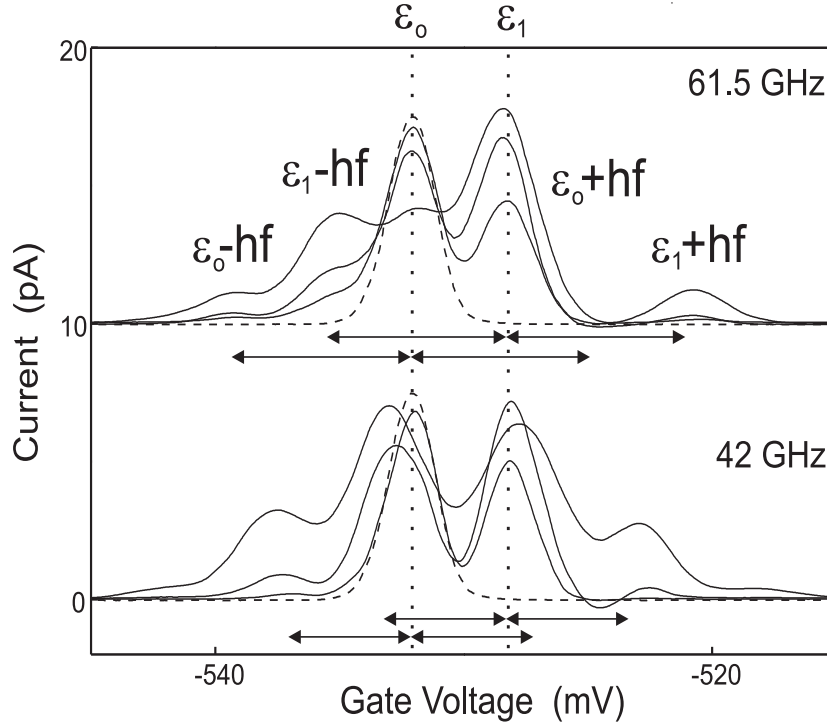


Figure 10. Measured current as a function of center gate voltage for different microwave powers. The dashed curve is without microwaves. $B = 0.91$ T, $V_{SD} = 13$ μ V. $f = 61.5$ GHz in the top section, $f = 42$ GHz in the bottom section. As the frequency is reduced between top and bottom sections, the ground-state resonance ε_0 and the resonance attributed to the excited state ε_1 remain at the same gate voltage position. The other peaks, $\varepsilon_0 - hf$ and $\varepsilon_1 \pm hf$, shift inward by an amount which corresponds to the change in photon energy as indicated by the arrows. We do not observe $\varepsilon_0 + hf$ in this measurement.

when we change the frequency, since the photon energy evidently does not alter the energy splitting. The other peaks, $\varepsilon_0 - hf$ and $\varepsilon_1 \pm hf$, shift by an amount that corresponds to the change in photon energy as indicated by the arrows. This reflects that the sidebands originate from matching the states ε_0 and ε_1 to the Fermi levels of the leads by a photon energy hf . Figure 11 shows a large data set. In each panel, different traces are taken at different microwave power. The panels differ in frequency. We further substantiate the peak assignment below by studying detailed frequency, magnetic field and power dependence.

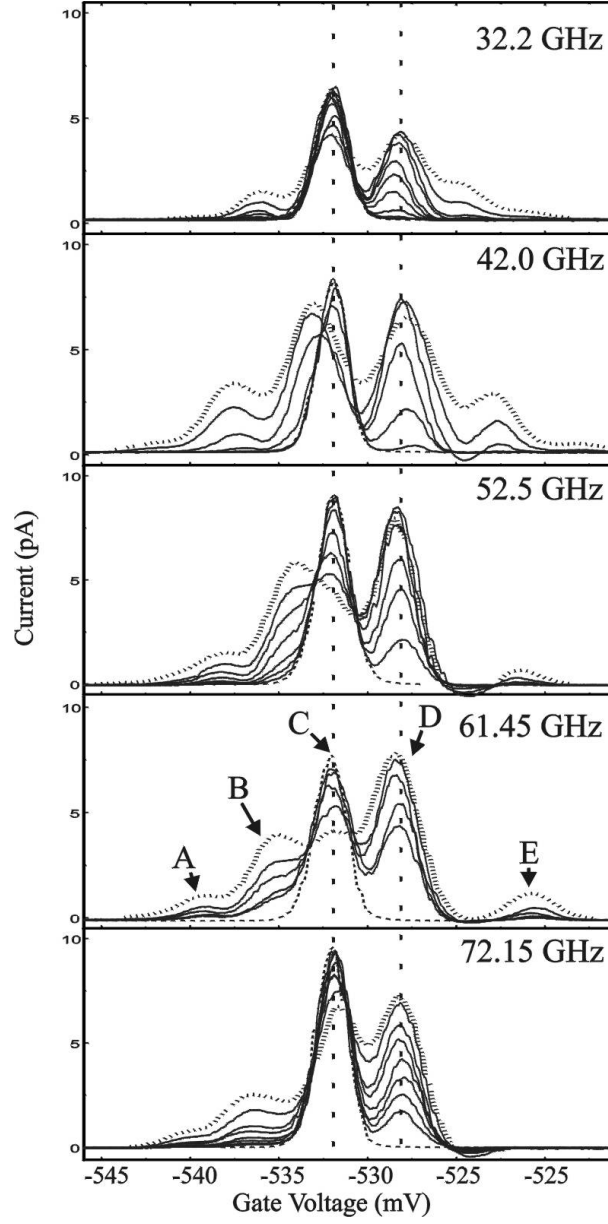


Figure 11. $I_{DC} - V_g$ curves for increasing frequency; $B = 0.91$ T, $V_{SD} = 13$ μ V and powers range between -30 and 0 dBm. The dashed curve is without microwave power. The dotted curve is with maximum power. Five different peaks can be distinguished in the data. These peaks, labelled A through E for the 61.45 GHz traces, correspond to the $\varepsilon_0 - hf$, $\varepsilon_1 - hf$, ε_0 , ε_1 and $\varepsilon_1 + hf$ peaks, respectively.

3.5. FREQUENCY DEPENDENCE

Figure 12 shows the spacing between a resonance and its photon sidebands as a function of the photon energy. Different markers correspond to different photon sidebands. The factor $\kappa = 35 \mu\text{eV}/\text{mV}$, to convert the peak spacings in mV gate voltage into energy, is determined from dc measurements. The full width at half maximum (FWHM) of the resonance without microwaves, indicated by the arrow, is proportional to the effective electron temperature in the leads. Structure due to photon energies below this value is washed out by the thermal energy $k_B T$. The frequency scaling firmly establishes PAT as the transport mechanism [9,11-14]. The observation that the sidebands move linearly with frequency, while the ground and excited state resonances stay fixed, supports our identification of the different peaks.

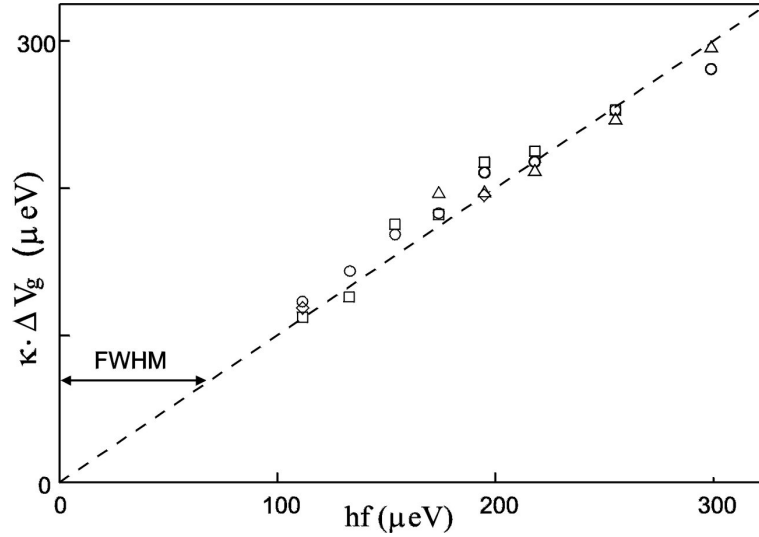


Figure 12. Peak spacings versus photon energy. □: spacing between ε_0 and $\varepsilon_0 - hf$. ◊: spacing between ε_0 and $\varepsilon_0 + hf$. △: spacing between ε_1 and $\varepsilon_1 - hf$. ○: spacing between ε_1 and $\varepsilon_1 + hf$. The dashed line is based on the gate voltage to energy conversion factor κ determined independently from dc measurements, and has the theoretically expected slope equal to 1. The arrow indicates the FWHM of the main resonance.

3.6. MAGNETIC FIELD DEPENDENCE

We now use a magnetic field to change the energy separation between the ground state and the first excited state [1, 36], while keeping the distance to the sidebands fixed. Figure 13a shows the positions in gate voltage of

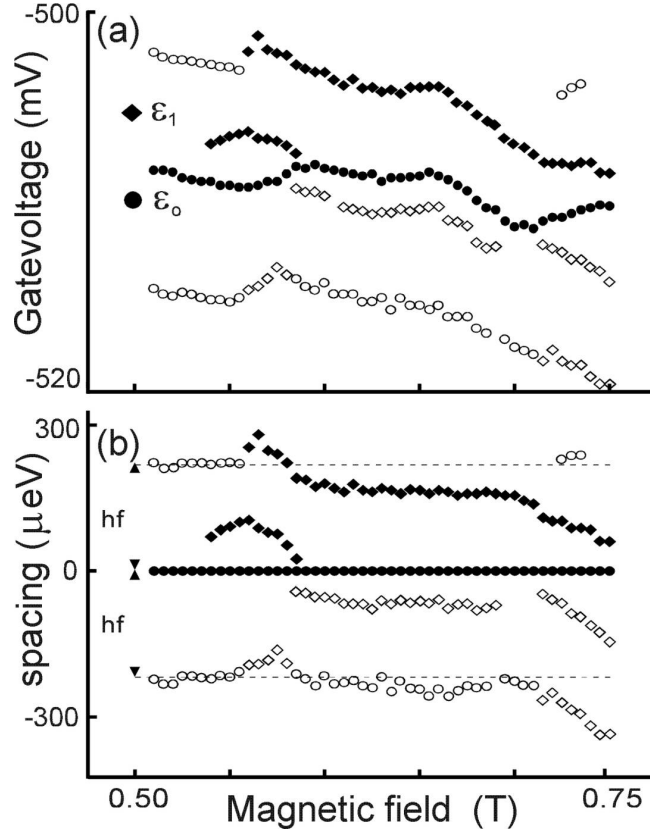


Figure 13. (a) Peak positions in gate voltage versus magnetic field at 52.5 GHz. Solid symbols denote peaks which are independent of frequency. Open symbols denote peaks that scale with frequency. (b) Peak spacings relative to the main resonance converted to energy. Closed circles: ϵ_0 ; open circles: $\epsilon_0 \pm hf$; closed diamonds: ϵ_1 ; open diamonds: $\epsilon_1 - hf$ and $\epsilon_1 - 2hf$.

all observed peaks for 52.5 GHz as a function of magnetic field. The filled circles reflect the evolution of ϵ_0 with magnetic field. This ground state weakly oscillates with a periodicity of ~ 80 mT which roughly corresponds to the addition of an extra flux quantum to the dot. The filled diamonds reflect the evolution of ϵ_1 . The open circles (diamonds) show the sidebands $\epsilon_0 \pm hf$ ($\epsilon_1 \pm hf$). Figure 13b shows the magnetic field evolution of the excited state and the photon sideband peaks relative to the ground state (i.e. we have subtracted $\epsilon_0(B)$ from the other curves). We see that the energy splitting decreases on increasing the magnetic field and for $0.54 \text{ T} < B < 0.58 \text{ T}$ a degeneracy of the ground state is temporarily lifted and

actually two excited states are observed [37]. The dashed lines denote the photon energy $hf = 217 \mu\text{eV}$ for 52.5 GHz. The open circles close to these lines are the photon processes $\varepsilon_0 \pm hf$, demonstrating that they indeed move together with the ground state. The open diamonds are the $\varepsilon_1 - hf$ and $\varepsilon_1 - 2hf$ processes. Their motion follows the motion of ε_1 . We have thus shown that we can vary the states ε_0 and ε_1 with the magnetic field and, independently, vary the separation to the sidebands with the microwave frequency.

3.7. POWER DEPENDENCE

Figure 14a shows a calculation of the peak heights as a function of the ac voltage drop across the barriers $\alpha = \frac{e\tilde{V}}{hf}$. Temperature, source-drain voltage, and frequency are taken from the experiment described below: $T = 200 \text{ mK}$, $V_{SD} = 13 \mu\text{V}$, and $f = 52.5 \text{ GHz}$. The tunnel rates from the leads to the ground state and the excited state are set to $\Gamma_{\varepsilon_0} = 5 \cdot 10^8 \text{ s}^{-1}$ and $\Gamma_{\varepsilon_1} = 14 \cdot 10^8 \text{ s}^{-1}$, respectively. The relaxation rate from the excited state to the ground state is assumed to be zero in the calculation. The effect of a finite relaxation rate is to reduce the height of ε_1 with respect to the other peaks. The calculated peak heights roughly follow the Bessel functions in Eq. (9). The ground-state resonance ε_0 follows $J_0^2(\alpha)$, since it involves only elastic tunnel events (see Fig. 4, diagram ε_0). The photon sidebands follow $J_1^2(\alpha)$, since they solely depend on the probability of photon absorption. For example, the process $\varepsilon_0 - hf$ is due to a photon assisted tunnel event which fills the dot. Once the dot is filled, however, it does not matter whether the dot is emptied via an elastic or an inelastic event. The process ε_1 follows the product of the Bessel functions $J_0^2(\alpha)J_1^2(\alpha)$ since it requires that the ground state is emptied via a PAT process, but also that the following tunneling processes through the excited state ε_1 are elastic.

Figure 14b shows the experimental results for the peak heights at $B = 0.91 \text{ T}$ and $f = 52.5 \text{ GHz}$ as a function of the ac voltage amplitude at the output of the source. The measurements are in good qualitative agreement below an ac source voltage of 100 mV. At higher ac voltages the pumped current starts to become important. The values for the tunnel rates to ε_0 and to ε_1 derived from the dc current-voltage characteristic are $\Gamma_{\varepsilon_0} = 5 \cdot 10^8 \text{ s}^{-1}$ and $\Gamma_{\varepsilon_1} = 6 \cdot 10^8 \text{ s}^{-1}$. The value for Γ_{ε_1} in the calculation is larger than the experimentally determined value, but still the calculated value for the height of the ε_1 resonance is smaller than the experimental value. It is a general trend in most of our data that the peak ε_1 is higher than predicted by our model and that $\varepsilon_0 + hf$ is lower than expected from simulations. A possible explanation has been put forward in Ref. [38].

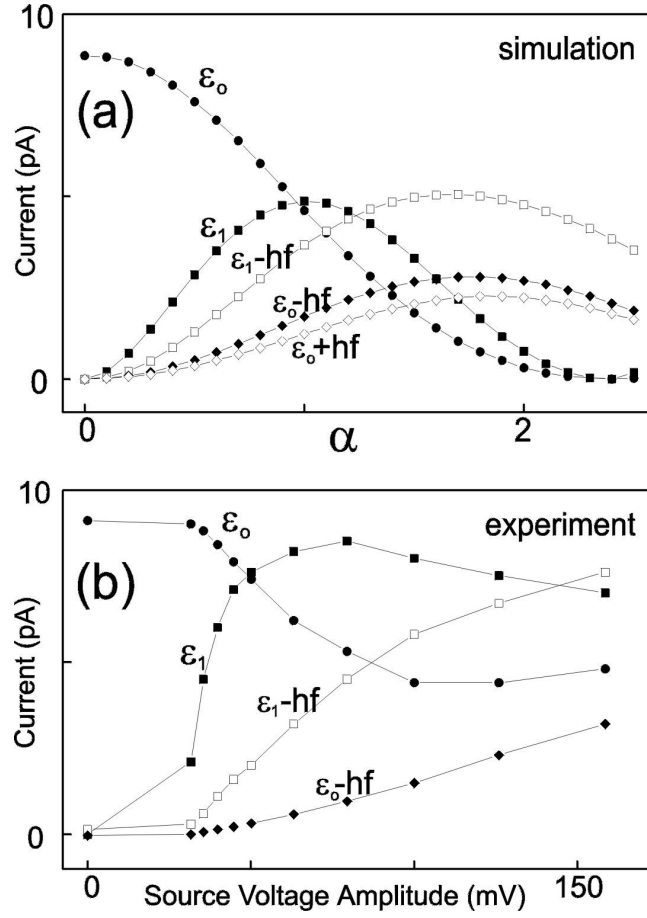


Figure 14. (a) Calculation of the peak heights as a function of the ac voltage drop across the barriers $\alpha = \frac{e\tilde{V}}{hf}$ ($T = 200$ mK, $V = 13$ μ V, $f = 52.5$ GHz). The tunnel rates from the leads to the ground state and the excited state are set to $\Gamma_{\epsilon_0} = 5 \cdot 10^8$ s $^{-1}$ and $\Gamma_{\epsilon_1} = 14 \cdot 10^8$ s $^{-1}$, respectively. The relaxation rate from the excited state to the ground state is assumed to be zero in the calculation. (b) Experimentally obtained peak heights as a function of the ac voltage amplitude (measured at the microwave source) for $V = 13$ μ V and $f = 52.5$ GHz.

3.8. DISCUSSION AND CONCLUSIONS

The simulations described earlier, show that the pumped current is quite independent of the bias voltage when $eV_{SD} \ll hf$, while current due to the photon resonances increases linearly with the bias voltage when $eV_{SD} < k_B T$. Therefore, it is possible to improve the quality of our data by

separating the pumped current from the photon resonances. This could be done by repeating a measurement at a particular microwave power for different bias voltages. In addition, the effective electron temperature of 200 mK reported here has now been improved to 50 mK. These two improvements would allow for a better comparison of future experiments with calculations over a wider range of microwave powers.

The conclusion of this work is that photon assisted tunneling is clearly observed in single-electron transport through small quantum dots. In addition, microwave irradiation can be used to perform spectroscopy on the discrete level spectrum. The parameter dependence of PAT is in reasonable agreement with calculations based on a master equation. Both, linear-frequency dependence and Bessel function power dependence are clearly observed. Recently, a non-equilibrium Green's function method applied to our PAT studies, has provided very good agreement with our results, including an explanation for the absence of the sideband at $\varepsilon_0 + hf$ [39]. Brune *et al.* [38] have analyzed the influence of intra-dot transitions. Including intra-dot transitions, they find good agreement with the height of the measured ε_1 peak in Figs. 10 and 11.

Qualitatively similar results have been obtained on superlattice structures irradiated by a free-electron laser. The dot and superlattice experiments have stimulated new theoretical interest in ac transport through non-superconducting structures. For instance, new results have been obtained for PAT across a single tunnel barrier for different sorts of oscillating potentials [40]; for PAT through superlattices in a self-consistent treatment [41], for the ac effects on transport through a QPC and double barrier structures in a numerical study [42], for the ac effects on correlated transport through Luttinger liquids [43], and for the Kondo effect in irradiated quantum dots [44].

These models and theories are very useful in explaining and predicting new transport mechanisms. We feel, however, that a word of caution is appropriate here. Although our PAT experiments give clean results, we have very little control over the oscillating potentials inside the sample. We simply couple in a microwave signal to one of the gates and measure the effect in the dc current. The dc response is very sensitive to the applied frequency. Sometimes the microwaves couple in more across the left barrier and sometimes more across the right barrier. The sensitivity of the asymmetry in coupling might be due to a complicated electric field pattern around the metallic gate structure. We think that to some degree our gate structure acts as a co-planar waveguide where the two QPC barrier gates serve as ground planes for the central microwave gate. Even under such conditions, it is not clear how this oscillating gate potential is carried over to the electron gas 100 nm below the surface. Pedersen and Büttiker [45]

have recently analyzed this problem for the case of quantum dots. They stress that oscillating potentials not only wiggle energy levels but also generate alternating currents in the sample. The alternating currents affect the self-consistent potential of the tunnel barriers and the potential on the dot. In effect, all the voltages and capacitances become renormalized and depend on the occupation of the dot. Sideband positions and heights are not expected to precisely follow a linear frequency dependence nor a Bessel function behavior. An experimental, quantitative study of the parameter dependence of the sidebands might give valuable information about these screening effects. Even more interesting would be to study the frequency dependence of the current, including measurements of higher harmonics at multiples of f . An analysis for such a set-up in terms of a frequency dependent environment is given in Ref. [46].

PAT is intrinsically a coherent phenomenon. The PAT measurements described above, however, are insensitive to the phase of the transmitted electrons. Coherence in the presence of a time-dependent field is therefore not directly demonstrated. Jauho and Wingreen [47] have proposed a PAT measurement through a quantum dot situated in one of two branches of an Aharonov-Bohm ring. They find that coherent absorption and reemission of photons can be detected via a phase measurement at the sidebands. The proposed mesoscopic double-slit geometry has been successfully used before to demonstrate coherent transmission through a quantum dot for the time-*independent* case [48, 49].

By connecting two quantum dots in series, a double quantum dot system can be obtained. An overview of charging effects in double quantum dots is given in Ref. [1]. Theoretical studies on PAT in a double quantum dot are done by Stoof and Nazarov [50], Stafford and Wingreen [51] and Brune *et al.* [52]. PAT studies of a double quantum dot enable the characterization of the coupling between two discrete energy levels. Depending on the strength of the inter-dot coupling, the two dots can form ‘ionic’ or ‘covalent’ bonds. By varying the inter-dot coupling, Oosterkamp *et al.* [53] experimentally demonstrated the transition from ionic bonding to covalent bonding in a quantum dot ‘artificial molecule’ that is probed by microwave excitations. In the same frequency regime experiments have been performed by Blick *et al.* [54] and by Fujisawa and Tarucha [15].

The study of photon assisted tunneling in quantum dots described here, forms a valuable extension of the understanding of the dc properties. Microwave measurements have been proved to be a useful spectroscopy tool for quantum dot systems. Microwaves are also expected to play a role of importance in future experiments on quantum dots and the possible application of quantum dots as solid state quantum bits. An example would be a time-resolved measurement of Rabi oscillations in a double quantum

dot. In this case, the microwave signal is used to tune the Rabi oscillation frequency [50, 51].

We thank R. Aguado, S.F. Godijn, A.E.A. Koolen, J.E. Mooij, Yu.V. Nazarov, R.M. Schouten, T. Fujisawa, S. Tarucha, T.H. Stoof, P. McEuen and N.C. van der Vaart for experimental help and useful discussions. This work was supported by the Dutch Organization for Research on Matter (FOM), by the EU via the TMR network (ERBFMRX CT98-0180), and by the NEDO joint research program (NTDP-98).

References

1. L.P. Kouwenhoven, C.M. Marcus, P.L. McEuen, S. Tarucha, R.M. Westervelt and N.S. Wingreen, in *Mesoscopic Electron Transport*, edited by L.L. Sohn, L.P. Kouwenhoven and G. Schön (Kluwer Dordrecht, Netherlands 1997), series E, vol. **345**, pp. 105-214; also available at <http://vortex.tn.tudelft.nl/~leok/papers>.
2. R. Ashoori, *Nature* **379**, 413-419 (1996).
3. L.P. Kouwenhoven, A.T. Johnson, N.C. van der Vaart, C.J.P.M. Harmans and C.T. Foxon, *Phys. Rev. Lett.* **67**, 1626 (1991); and *Zeitschrift für Physik* **85**, 381 (1991).
4. U. Merkt, *Physica B* **189**, 165 (1993) and references therein.
5. R. Strenz, U. Bockelmann, F. Hirler, G. Abstreiter, G. Böhm and G. Weimann, *Phys. Rev. Lett.* **73**, 3022 (1994) and references therein.
6. K. Brunner, G. Abstreiter, G. Böhm, G. Tränkle and G. Weimann, *Phys. Rev. Lett.* **73**, 1138 (1994).
7. L. Jacak, P. Hawrylak and A. Wojs, *Quantum Dots* (Springer-Verlag Berlin Heidelberg 1998).
8. J.R. Tucker and M.J. Feldman, *Rev. Mod. Phys.* **57**, 1055 (1985).
9. P.K. Tien and J.R. Gordon, *Phys. Rev.* **129**, 647 (1963).
10. High frequency studies on quantum wells and quantum point contacts have not shown discrete photon features. See for microwave studies on quantum wells: V.A. Chitta, C. Kutter, R.E.M. de Bekker, J.C. Maan, S.J. Hawskworth, J.M. Chamberlain, M.Henini and G. Hill, *J.Phys.: Condens. Matter* **6**, 3945 (1994), and references therein. See for microwave studies on quantum point contacts: R.A. Wyss, C.C. eugster, J.A. del Alamo and Q. Hu, *Appl. Phys. Lett.* **63**, 1522 (1993); T.J.B.M. Janssen, J.C. Maan, J. Singleton, N.K. Patel, M. Pepper, J.E.F. Frost, D.A. Ritchie and G.A.C. Jones, *J.Phys.: Condens. Matter* **6**, L163 (1994).
11. P.S.S. Guimarães, B.J. Keay, J.P. Kaminski, S.J. Allen, Jr., P.F. Hopkins, A.C. Gossard, L.T. Florez and J.P. Harbison, *Phys. Rev. Lett.* **70**, 3792 (1993); B.J. Keay, S.J. Allen, Jr., J. Galán, J.P. Kaminski, K.L. Campman, A.C. Gossard, U. Bhattacharya and M.J.W. Rodwell, *Phys. Rev. Lett.* **75**, 4098 (1995); B.J. Keay, S. Zeuner, S.J. Allen, Jr., K.D. Maranowski, A.C. Gossard, U. Bhattacharya and M.J.W. Rodwell, *Phys. Rev. Lett.* **75**, 4102, (1995).
12. L.P. Kouwenhoven, S. Jauhar, K. McCormick, D. Dixon, P.L. McEuen, Yu. V. Nazarov, N.C. van der Vaart, and C.T.Foxon, *Phys. Rev. B* **50**, 2019 (1994).
13. L.P. Kouwenhoven, S. Jauhar, J. Orenstein, P.L. McEuen, Y. Nagamune, J. Motohisa and H. Sakaki, *Phys. Rev. Lett.* **73**, 3433 (1994).
14. R.H. Blick, R.J. Haug, D.W. van der Weide, K. von Klitzing, and K. Eberl, *Appl. Phys. Lett.* **67**, 3924 (1995).
15. T. Fujisawa and S. Tarucha, *Superlattices Microstructures* **21**, 247 (1997).

16. T.H. Oosterkamp, L.P. Kouwenhoven, A.E.A. Koolen, N.C. van der Vaart and C.J.P.M. Harmans, Phys. Rev. Lett. **78**, 1536-1539 (1997).
17. M. Büttiker and R. Landauer, Phys. Rev. Lett. **49**, 1739 (1982).
18. M. Switkes, C.M. Marcus, K. Campman, and A.C. Gossard, to be published in Science, (March 1999).
19. Mixing is described by J. Iñarrea, G. Platero and C. Tejedor, Phys. Rev. B **50**, 4581 (1994).
20. D. Sokolovski, Phys. Rev. B **37**, 4201 (1988).
21. P. Johansson, Phys. Rev. B **41**, 9892 (1990).
22. *Single Charge Tunneling*, edited by H. Grabert and M. Devoret (Plenum Press London 1992), series B, vol. **294**.
23. D.V. Averin, A.N. Korotkov and K.K. Likharev, Phys. Rev. B **43**, 6199 (1991).
24. C.W.J. Beenakker, Phys. Rev. B **44**, 1646 (1991).
25. K.K. Likharev and I.A. Devyatov, Physica B **194-196**, 1341 (1994).
26. A. Hadicke and W. Krech, Physica B **193**, 256 (1994).
27. C. Bruder and H. Schoeller, Phys. Rev. Lett. **72**, 1076 (1994).
28. For a review see: G.L. Ingold and Yu. V. Nazarov, p. 21 in Ref. [22].
29. G.Y. Hu and R.F. O'Connell, Phys. Rev. B **49**, 16505 (1994).
30. J.M. Hergenrother, M.T. Tuominen, J.G. Lu, D.C. Ralph and M. Tinkham, Physica B **203**, 327 (1994).
31. T. Fujisawa, T.H. Oosterkamp, W.G. van der Wiel, B.W. Broer, R. Aguado, S. Tarucha and L.P. Kouwenhoven, Science **282**, 932-935(1998).
32. T.H. Oosterkamp, L.P. Kouwenhoven, A.E.A. Koolen, N.C. van der Vaart and C.J.P.M. Harmans, Semiconductor Science and Technology **11**, 1512 (1996); T.H. Oosterkamp, L.P. Kouwenhoven, A.E.A. Koolen, N.C. van der Vaart, and C.J.P.M. Harmans, Physica Scripta T**69**, 98 (1997).
33. J.-C. Wan, K.A. McGreer, L.I. Glazman, A.M. Goldman and R.I. Shekhter, Phys. Rev. B **43**, 9381 (1991).
34. PAT is also observed at $B = 0$ but with less resolution due to a higher effective electron temperature at $B = 0$.
35. Because $2\hbar f > \Delta\varepsilon$ the excited state ε_1 is weakly visible at $V_g \sim -508$ mV in Fig. 9 where it overlaps with $\varepsilon_0 + 2\hbar f$.
36. A.T. Johnson, L.P. Kouwenhoven, W. de Jong, N.C. van der Vaart, C.J.P.M. Harmans and C.T. Foxon, Phys. Rev. Lett. **69**, 1592 (1992).
37. Our measurement of the evolution of the excited state ε_1 agrees with the data in Fig. 4 of Ref. [36] and in Fig. 11 of P.L. Mc Euen *et al.*, Physica B **189**, 70 (1993). However, we do not know of a theory that properly describes the observed magnetic field dependence of excited states.
38. Ph. Brune, C. Bruder and H. Schoeller, Phys. Rev. B **56**, 4730 (1997).
39. Q. Sun, J. Wang and T. Lin, Phys. Rev. B **58**, 13007 (1998).
40. M. Wagner and W. Zwerger, Phys. Rev. B **55**, 10217 (1997), and references therein.
41. R. Aguado and G. Platero, Phys. Rev. Lett. **81**, 4971 (1998).
42. K. Yakubo, S. Feng and Q. Hu, Phys. Rev. B **54**, 7987 (1996).
43. G. Cuniberti, M. Sassetti and B. Kramer, Phys. Rev. B **57**, 1515 (1998).
44. R. López, R. Aguado, G. Platero and C. Tejedor, Phys. Rev. Lett. **81**, 4688 (1998), and references therein.
45. M.H. Pedersen and M. Büttiker, Phys. Rev. B **58**, 12993 (1998).
46. R. Aguado and L.P. Kouwenhoven, Phys. Rev. Lett. **84**, 1986-1989 (2000).
47. A.P. Jauho and N.S. Wingreen, Phys. Rev. B **58**, 9619 (1998).

- 48. A. Yacoby, M. Heiblum, D. Mahalu and H. Strikman, Phys. Rev. Lett. **74**, 4047 (1995).
- 49. R. Schuster, E. Buks, M. Heiblum, D. Mahalu, V. Umansky and H. Strikman, Nature **385**, 417 (1997).
- 50. T.H. Stoof and Yu.V. Nazarov, Phys. Rev. B **53**, 1050-1053 (1996).
- 51. C.A. Stafford and N.S. Wingreen, Phys. Rev. Lett. **76**, 1916-1919 (1996).
- 52. Ph. Brune, C. Bruder and H. Schoeller, Physica E **1**, 216-218 (1997).
- 53. T.H. Oosterkamp, T. Fujisawa, W.G. van der Wiel, K. Ishibashi, R.V. Hijman, S. Tarucha and L.P. Kouwenhoven, Nature **395**, 873 (1998).
- 54. R.H. Blick, R. J. Haug, J. Weis, D. Pfannkuche, K. v. Klitzing and K. Eberl, Phys. Rev. B **53**, 7899-7902 (1996); R.H. Blick, D.W. van der Weide, R.J. Haug and K. Eberl, Phys. Rev. Lett. **81**, 689 (1998).

